

In-Plane Ferroelectricity in Thin Flakes of Van der Waals Hybrid Perovskite

Lu You, Fucai Liu, Hongsen Li, Yuzhong Hu, Shuang Zhou, Lei Chang, Yang Zhou, Qundong Fu, Guoliang Yuan, Shuai Dong, Hong Jin Fan, Alexei Gruverman, Zheng Liu,* and Junling Wang*

Collective ferroic orders in van der Waals (vdW) crystals are receiving increasing attention in 2D materials research. The interplay between spatial quantum confinement and long-range cooperative phenomena not only broadens the horizon of fundamental physics, but also enables new device paradigms and functionalities built upon vdW heterostructures. Here, the in-plane ferroelectric properties in thin flakes of vdW hybrid perovskite bis(benzylammonium) lead tetrachloride are studied. The ordering of electric dipoles along the layer plane circumvents the depolarization field and preserves the ferroelectricity down to one unit-cell thickness or two vdW layers at room temperature. The superior performance of the electromechanical energy conversion is demonstrated by exploiting its in-plane piezoelectricity. The successful isolation of ferroelectric order in atomically thin vdW hybrid perovskite paves the way for nonvolatile flexible electronic devices with the cross-coupling between strain, charge polarization, and valley degrees of freedom.

A key question is whether the long-range order can survive against the formidable destabilizing field and thermal fluctuation when the ferroic material approaches 2D limit. For example, dimension/size effect is notorious for ferroelectric ultrathin films due to the suppression of ferroelectricity by depolarization effect.^[5] In conventional 3D ferroelectric heterostructures, the interfacial bonding and charge mismatch can play a deterministic role in the stability and switchability of the polarization.^[6,7] In contrast, van der Waals (vdW) ferroelectrics exhibit much weaker interaction between layers and with the supporting substrate. By employing sufficiently conductive electrodes, it was previously shown that ferroelectricity can be sustained down to few-layer thickness in a vdW ferroelectric material with out-of-plane polarization.^[8] Another way to circumvent the depolarization effect is to explore ferroelectrics with in-plane polarization.^[9] One of the

Despite their fundamental and technological significance, ferroic orders in 2D materials, such as ferroelectricity, ferromagnetism, and ferroelasticity, remain largely unexplored.^[1–4]

Dr. L. You, Prof. H. Li, Dr. S. Zhou, L. Chang, Dr. Y. Zhou, Prof. J. Wang
School of Materials Science and Engineering
Nanyang Technological University
Singapore 639798, Singapore
E-mail: jlwang@ntu.edu.sg

Dr. F. Liu
School of Optoelectronic Science and Engineering
University of Electronic Science and Technology of China
Chengdu 610054, P. R. China

Dr. F. Liu, Q. Fu, Prof. Z. Liu
Centre for Programmable Materials
School of Materials Science and Engineering
Nanyang Technological University
Singapore 639798, Singapore
E-mail: z.Liu@ntu.edu.sg

Prof. H. Li
School of Chemistry and Chemical Engineering
Shanghai University of Engineering Science
Shanghai 201620, P. R. China

Y. Hu, Prof. H. J. Fan
School of Physical and Mathematical Sciences
Nanyang Technological University
Singapore 637371, Singapore


Dr. S. Zhou
School of Science
Nanjing University of Posts and Telecommunications
Nanjing 210023, P. R. China

Prof. G. Yuan
School of Materials Science and Engineering
Nanjing University of Science and Technology
Nanjing 210094, P. R. China

Prof. S. Dong
School of Physics
Southeast University
Nanjing 211189, P. R. China

Prof. A. Gruverman
Department of Physics and Astronomy
University of Nebraska-Lincoln
Nebraska 68588, USA

Prof. J. Wang
Academy for Advanced Interdisciplinary Studies
and Department of Physics
Southern University of Science and Technology
Shenzhen 518055, P. R. China

 The ORCID identification number(s) for the author(s) of this article can be found under <https://doi.org/10.1002/adma.201803249>.

DOI: 10.1002/adma.201803249

candidate compounds is the Ruddlesden–Popper (RP) family ($A_{n+1}B_nX_{3n+1}$), in which the 3D ABX_3 perovskite blocks are sliced into layered slabs by inserting an extra AX layer per n perovskite unit cells.^[10,11] Specifically in organic–inorganic hybrid perovskites ($(RNH_3)_2A_{n-1}B_nX_{3n+1}$), A- and B-site cations and X anions form the 3D perovskite network, while the large RNH_3^+ groups act as the spacers between the perovskite layers with weak vdW bonds.^[12] The $n = 1$ compound thus represents the simplest layered structure, in which ferroelectricity arises from the horizontal off-center ordering of the RNH_3^+ molecule with respect to the inorganic framework. Hence, the polarization is confined within one crystal layer, and separated by the vdW gap between different layers. Owing to the weak interlayer yet strong intra-layer bonds, ferroelectric/piezoelectric vdW crystals can be easily downscaled to ultrathin level with large mechanical flexibility and strength on arbitrary substrates, which makes them highly promising for mechanical energy harvesting and flexible electromechanical applications at nanoscale.^[13,14] Moreover, the coexistence of strong spin-orbit coupling and ferroelectricity in lead halide-based perovskite may enable electrical control of the Rashba spin splitting through ferroelectric polarization switching and open up novel device paradigms in 2D valleytronics by incorporating the ferroic order parameters.^[15,16]

However, the stability of the ferroelectric order in atomically-thin hybrid vdW ferroelectrics remains unclear.

In this study, we report the observation of in-plane ferroelectricity in bis(benzylammonium) lead tetrachloride (BA_2PbCl_4) down to one unit cell or two vdW layers at room temperature. Switching characteristics of the ferroelectric domains in this hybrid compound are investigated in details. Finally, a flexible device based on its piezoelectricity is demonstrated, which opens up possible applications of the vdW hybrid perovskites in nanoscale electromechanical energy conversions, such as energy harvesting and sensing.

As shown in **Figure 1b**, the high temperature phase of BA_2PbCl_4 is centrosymmetric, with twofold orientational disorder of the benzylammonium cation. Below Curie temperature ($T_C \approx 453$ K), the organic cation is frozen in one of the two off-center positions, resulting in a relative displacement with respect to the negatively charged $PbCl_6$ octahedron and net in-plane polarization that can be switched by an external electric field.^[10] Meanwhile, Pb^{2+} cation is also displaced from the octahedral center along the polar axis, which contributes additionally to the total polarization (Figure S1, Supporting Information). Therefore, the BA_2PbCl_4 has a mixed character of displacive- and order-disorder-type ferroelectrics. Thanks to

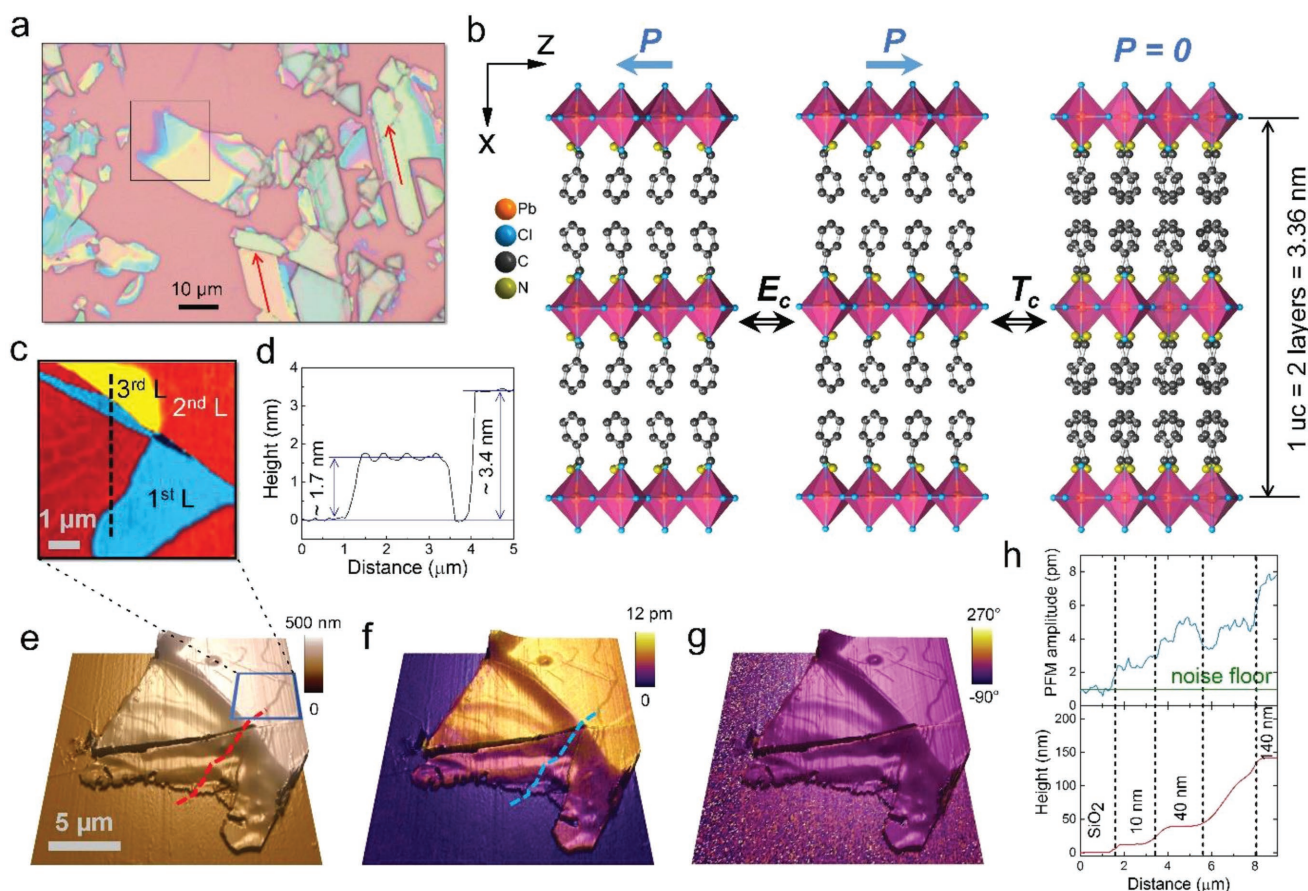


Figure 1. Crystal structure and characterizations of BA_2PbCl_4 flakes. a) Typical optical image of BA_2PbCl_4 flakes exfoliated on SiO_2 -coated Si substrate with various color contrasts and thicknesses. b) Atomic structures of BA_2PbCl_4 below T_C with switchable polarization and above T_C with no spontaneous polarization. c) Surface topography of the BA_2PbCl_4 flake as defined by the blue box in (e). d) Height profile along the black dash line in (c) showing monolayer steps. e) Height, f) PFM amplitude, and g) PFM phase signals overlaid on 3D surface topography of the BA_2PbCl_4 flake as indicated by the black box in (a). h) Correlated height and PFM amplitude profiles along the dash lines denoted in (e) and (f).

the weak interlayer vdW interaction, single crystals of BA_2PbCl_4 can be readily exfoliated onto various substrates using the Scotch tape method.^[17] The phase purity and crystallinity of the BA_2PbCl_4 single crystal were examined using X-ray diffraction (XRD), Fourier-transform infrared spectroscopy (FTIR), and confocal Raman spectroscopy (Figure S2, Supporting Information). A typical optical micrograph of the exfoliated flakes is shown in Figure 1a. Topographic image of the thin flake (Figure 1c,d) displays sharp atomic steps that correspond to the thickness of one crystal layer (≈ 1.7 nm). Note that a complete unit cell consists of two crystal layers in ferroelectric BA_2PbCl_4 . We then employed lateral piezoelectric force microscopy (PFM) to study the nanoscale ferroelectric properties. Shown in Figure 1e–g are the 3D topographic image and the corresponding PFM amplitude and phase images overlaid on top of it, respectively. The BA_2PbCl_4 flake exhibits clear piezoelectric response compared with the SiO_2 -coated Si substrate in the amplitude channel, while the uniform phase contrast indicates a single-domain state. The associated topographic and PFM line sections reveal that the piezoresponse decreases with reduced flake thickness, but it remains well above noise floor even for the 10 nm thick flake. The PFM amplitude shows a linear relationship with the applied AC driving voltage, confirming the intrinsic piezoresponse (Figure S3c, Supporting Information).

The lateral PFM detects the torsional motion of the atomic force microscope (AFM) cantilever induced by the shear piezoelectric effect (piezoelectric coefficient d_{xs}) arising from the nonzero in-plane polarization $P_{||}$ (Figure S3, Supporting Information). The piezoresponse signal is thus proportional to $P_{||}\sin\phi$, where ϕ is the azimuthal angle between the cantilever axis and in-plane polarization vector. Next, we performed angular-resolved PFM by rotating the sample with respect to the cantilever axis to determine the polarization vector of the BA_2PbCl_4 flake (Figure 2a). Particularly, dual AC resonance tracking (DART) method was used to enhance the signal-to-noise ratio and the results are fitted using the simple harmonic oscillator (SHO) model, from which the quantitative piezoresponse amplitude A , phase θ , quality factor Q , and first resonant frequency f can be derived (Figure S4, Supporting Information).^[18]

Figure 2b shows the corresponding PFM images and the polar plot of the piezoresponse amplitude data for various sample-cantilever azimuth angles. Herein, the PFM images are displayed using combined amplitude and phase signals, namely, $A\cos\theta$ ($\theta = 0$ or π), in which the absolute value represents the magnitude of the piezoresponse, while the sign denotes the polarization direction. By fitting the angular-dependent amplitude and phase signals, the in-plane polarization axis of the BA_2PbCl_4 flake can be determined, as labeled by the arrows in Figure 2b and those in Figure 1a. It can be found that the polar axis coincides with some of the regular cleavage edges. Due to zero polarization along vertical direction, there is no piezoresponse in the out-of-plane PFM image except for the buckling crosstalk induced by the in-plane polarization component along the cantilever axis (Figures S3 and S5, Supporting Information).^[19]

Upon reducing the thickness of the BA_2PbCl_4 flakes, the key question is if the ferroelectric order can survive thermal fluctuation in the atomically thin limit, since ferroelectricity is a collective order parameter that involves interlayer interactions in bulk. In Figure 3, we show the robust room-temperature ferroelectricity in BA_2PbCl_4 flakes with single-unit-cell thickness, that is, two crystal layers. The edge of the flakes exhibits significant material degradation, possibly due to the high ambient humidity. However, by the correlation between topographic and PFM line profiles, the single-unit-cell flake demonstrates strong piezoelectric response, whose phase signal can be reversed by rotating the sample by 180° . This observation suggests that the in-plane ferroelectricity can be sustained down to atomically thin limit, and the weak interlayer interaction has little effect on the long-range ordering of the electric dipoles in this material. To quantitatively assess the piezoelectric coefficient of the BA_2PbCl_4 flakes, we carefully calibrate the torsional optical lever sensitivity and double-check the PFM response in both off-resonance and resonance-enhanced modes. The results are summarized in Figure S6 in the Supporting Information for different flake thicknesses and on both insulating and conductive substrates. Overall, the effective d_{15} measured on conductive substrate is higher than that on insulating substrate. This is because the applied voltage will drop more effectively across

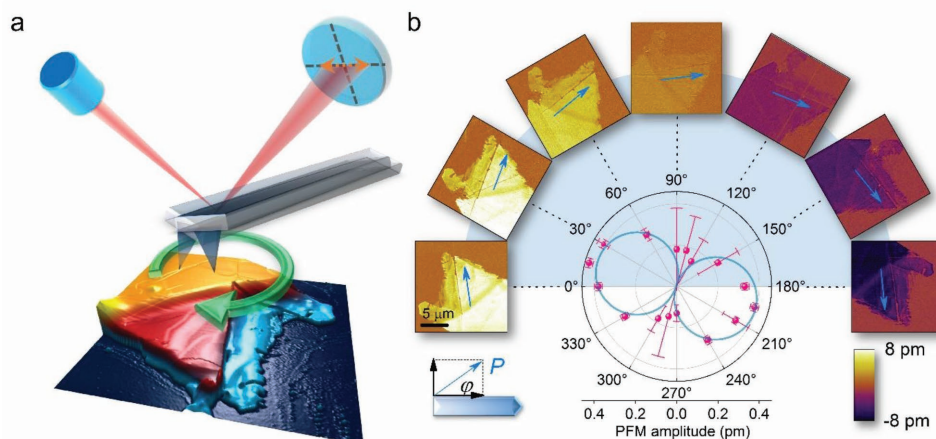


Figure 2. Angular-resolved PFM study of BA_2PbCl_4 flakes. a) Schematic of the experimental setup. b) Angular-resolved PFM images of BA_2PbCl_4 flakes at different azimuth angles, ϕ . The effective piezoresponse data after SHO fit and correction are plotted in polar coordinate, in which the distance from the origin represents the amplitude. The blue solid line is a cosine function fit. The blue arrow denotes the identified polarization vector.

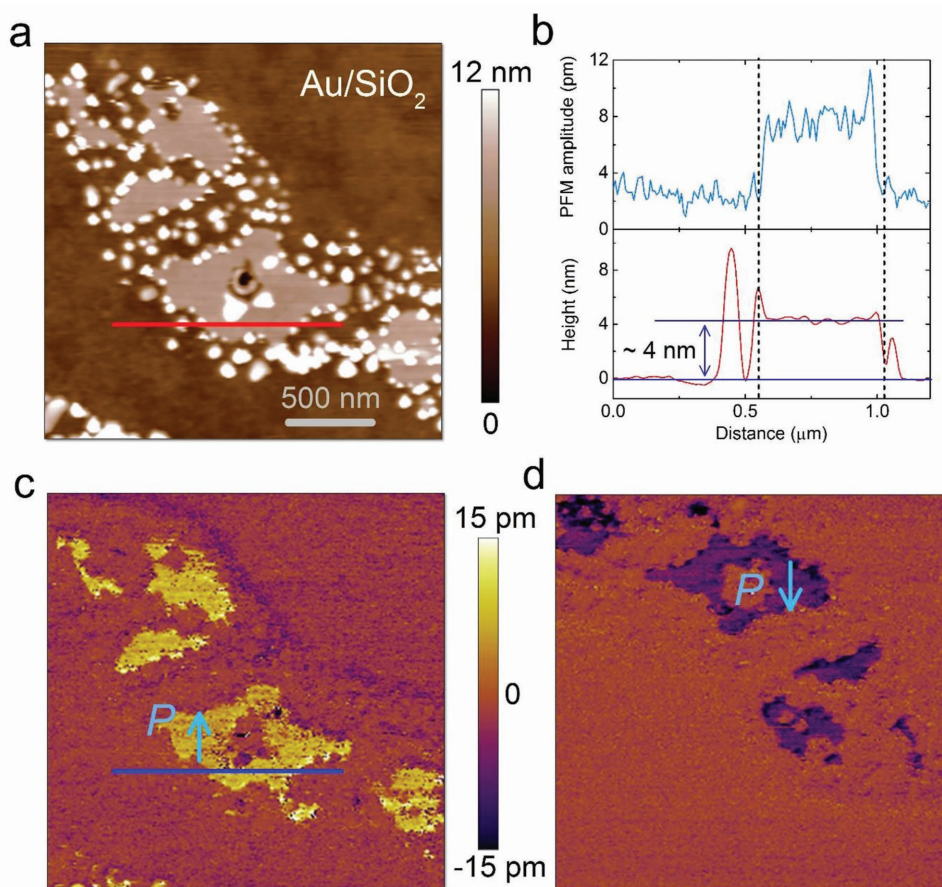


Figure 3. Room-temperature ferroelectricity in single-unit-cell BA_2PbCl_4 . a) Topographic image of single-unit-cell BA_2PbCl_4 flakes. b) Correlated height and PFM amplitude profiles along the solid lines in (a) and (c). c, d) Lateral PFM images of single-unit-cell BA_2PbCl_4 flakes with reversed sample orientations.

the sample thickness on conductive substrate. Obviously, the thickness-dependent piezoresponse doesn't follow the scaling law typically found in vertical PFM,^[20] where a critical thickness exists due to the overwhelming depolarization field in the ultrathin limit. This is consistent with the fact that the depolarization field is strongly alleviated when the polarization lies in the plane. Nevertheless, the piezoresponse still decreases rapidly in ultrathin region. This can be explained by the smaller effective field in ultrathin flake when a dielectric gap or dead layer in between the tip and sample is considered. Another possible factor is that the clamping effect by the surrounding film also increases with reduced thickness. We can estimate an upper bound of the d_{15} to be around 1 pm V^{-1} . This value is much smaller than those of typical oxide ferroelectrics,^[21] which implies that the 2D layered structure imposes strong geometric confinement on the polarization dipole, making it highly difficult to rotate.

To test the switchability of the ferroelectric polarization, in-plane electric field was applied to a BA_2PbCl_4 flake using co-planar electrodes, as shown in Figure 4a. Starting with a single-domain state, polarization reversal is achieved through classical switching process that includes domain nucleation, forward growth, and sideways growth (Figure S7, Supporting Information). The majority of the domain switches within a narrow window of the voltage range, indicating the

homogeneity of the crystal. The opposite domain then forms two charged domain boundaries with the preexisting domains. However, they exhibit very different domain wall roughness. The negatively charged wall is very flat and smooth, while the positively charged one is highly rough with zigzag pattern. Scanning Kelvin probe microscopy (SKPM) was then used to map out the surface potential of the same area (Figure 4b). Unexpectedly, both domain boundaries show bright contrast in the SKPM image, suggesting positive charges. The positive charges can thus be understood as excessive holes injected from the electrode, which stabilize the negatively charged wall.^[22,23] However, little electrons were injected from the other side, and there are no sufficient free electrons in the crystal. This makes the positively charged wall very energetic, which takes the zigzag form to minimize the electrostatic energy.

The local polarization switching can also be achieved using the stray field from a biased AFM probe.^[24,25] In Figure 4c, the biased AFM probe was scanned along the dotted arrow, generating radial field that may switch the proximate domains. As the probe was positively biased, it produced a line of negatively charged wall. A small portion of positively charged wall was also created. However, similar to the co-planar electrode case, the positively charged wall seems highly unstable, which quickly diminishes within minutes once created, leaving only negatively charged wall. Based on these observations, we can

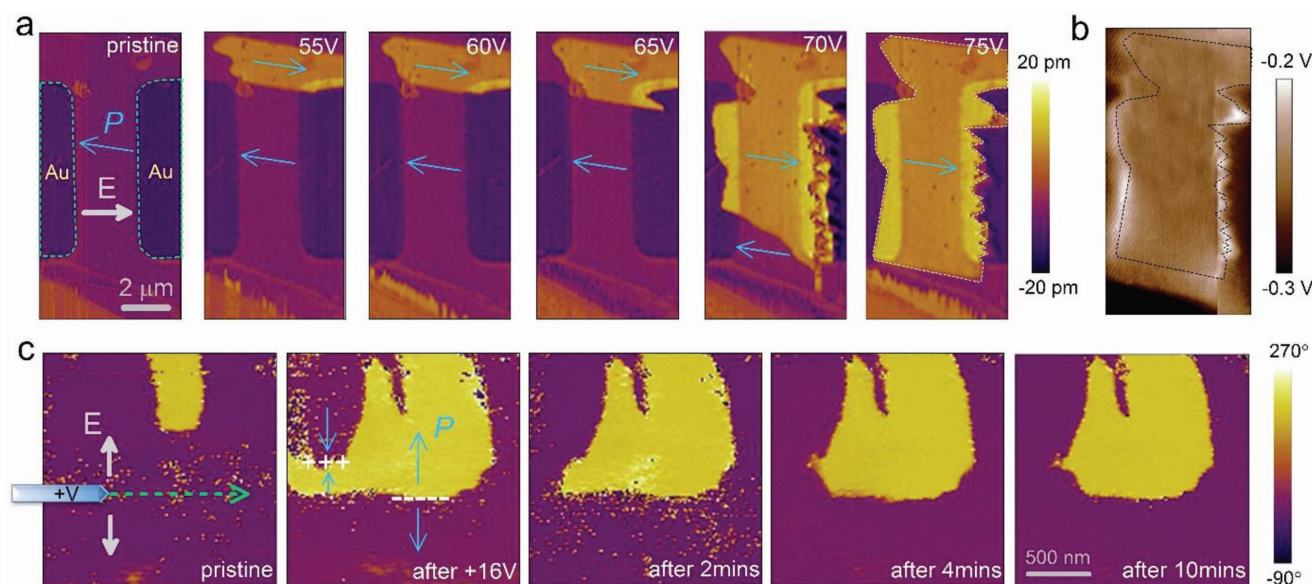


Figure 4. Ferroelectric switching of BA_2PbCl_4 . a) Lateral PFM images during the polarization switching of a 50 nm thick BA_2PbCl_4 flake using co-planar electrodes. A square pulse of 1 ms width was applied to the sample with increasing magnitude (55–75 V) at 5 V interval. b) SKPM image taken right after the 75 V pulse shown in (a). c) Lateral PFM phase images during the polarization switching of a 40 nm thick BA_2PbCl_4 flake using the scanning probe. After switching the sample by applying 16 V to the probe, the ferroelectric domain gradually relaxed to its equilibrium state with time. The polarization directions in (a) and (c) are indicated by the blue arrows.

infer that the majority free carrier in the BA_2PbCl_4 is hole, which favors the formation of negatively charged walls rather than the positively charged ones. Additionally, interdigitated electrode was also fabricated on the surface of the BA_2PbCl_4 crystal to measure the macroscopic polarization hysteresis loops (Figure S8, Supporting Information).

The 2D layered structure endows BA_2PbCl_4 great advantage in flexible applications. By exploiting its piezoelectricity, we fabricated a two-terminal device on a flexible polyethylene terephthalate (PET) substrate. Bending the substrate exerts tensile/compressive strain on the BA_2PbCl_4 flake atop, generating piezoelectric current in short-circuit condition, as shown in Figure 5a. Upward and downward bending produces opposite signs of the current. During the measurements, special care has been taken to eliminate the parasitic effects (Figure S9, Supporting Information).^[26] Due to the different time durations of the manual bending and releasing actions, the peak currents are not symmetric. However, the integrated charges are almost identical, indicating the reversible piezoelectric effect (Figure 5b). Based on the geometry of the device and bending condition, we can estimate that the applied strain ϵ_{zz} is ≈ 0.02 (Figure S10 and Text S1, Supporting Information). The longitudinal piezoelectric coefficient e_{33} can then be deduced by

$$e_{33} = \left(\frac{\partial P_z}{\partial \epsilon_{zz}} \right)^E \quad (1)$$

where P_z is the polarization induced by the external strain along z direction. P_z is calculated, by dividing the generated charge by the cross-sectional area of the BA_2PbCl_4 flake, to be $\approx 0.04 \text{ C m}^{-2}$. The e_{33} of BA_2PbCl_4 can thus be estimated to be around 2 C m^{-2} , much higher than the piezoelectric MoS_2 ^[27] and other 2D layered materials.^[28,29]

Compared to 3D ferroelectric materials with in-plane polarization,^[9] the 2D hybrid perovskites show much weaker thickness-dependent ferroelectric order due to their weak interlayer interactions. The confinement of the electron wave functions also makes less interactive with the supporting substrate, alleviating the interface effect. The demonstration of robust room-temperature ferroelectricity in thin flakes of vdW hybrid perovskite holds great significance and possibilities for multiple research fields. For example, the polar order and its influence on the optical physics in 3D lead halide perovskites remains an intensively debated topic. Though theoretically predicted,^[30–33] unambiguous experimental proofs of their ferroelectricity are still elusive.^[34–42] It is now possible to combine BA_2PbCl_4 and methylammonium lead chloride (MAPbCl_3) to form a series of RP phases by continuously tuning the lattice dimensionality from 2D to 3D limit. It is then intriguing to see whether the ferroelectric ground state can be stabilized by sandwiching 3D MAPbCl_3 with 2D BA_2PbCl_4 , and how the electric dipole ordering may affect the photocarrier dynamics and photovoltaic response in these homologous compounds.^[43–45] Furthermore, the coexistence of inversion symmetry breaking, strong spin-orbit coupling, and 2D nature combines the Rashba splitting and valley-dependent spin polarization in BA_2PbCl_4 , both of which can become electrically switchable since they are inherently coupled to the spatial inversion of the lattice.^[15,46] This unique characteristic may lead to innovative devices for non-volatile information processing and storage.^[47,48] BA_2PbCl_4 is a direct bandgap semiconductor, but with a large energy gap of 3.65 eV^[10] due to the strong ionic character of the Pb–Cl bond. However, it is possible to redshift the bandgap to the visible range by exploring the bromide and iodide counterparts with various aliphatic or aromatic alkylamine groups and metal cations.^[11,49,50] This will greatly facilitate the accessibility to its

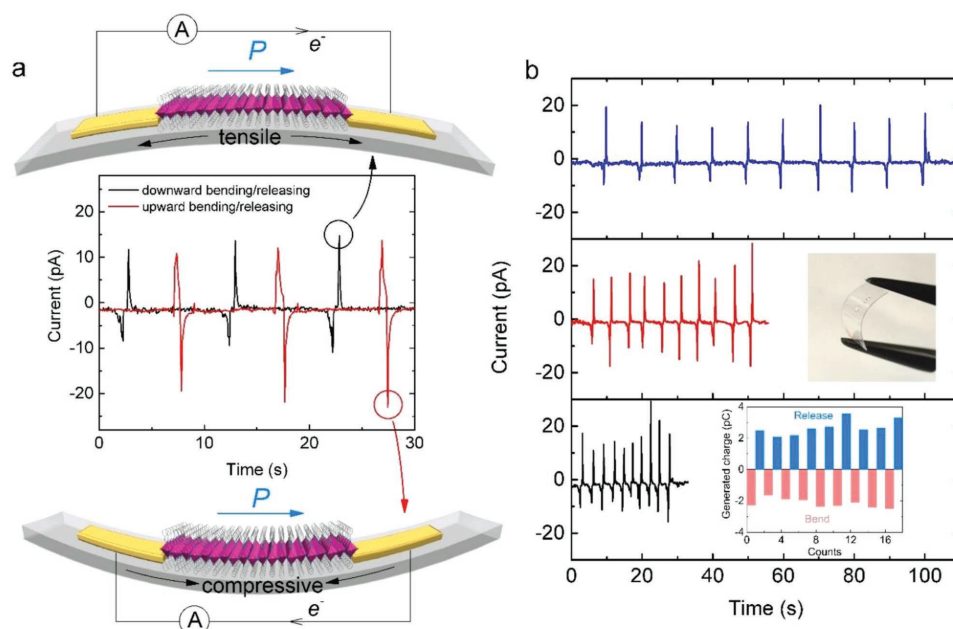


Figure 5. Flexible electromechanical device based on BA_2PbCl_4 . a) Representative current responses under downward and upward bending/releasing cycles. The upper and lower panels show the device schematics. b) Current responses under downward bending/releasing cycles with different time intervals. The inset of the middle panel pictures a transparent flexible $\text{BA}_2\text{PbCl}_4/\text{PET}$ device. The inset of the lower panel illustrates the generated charge for every bending/releasing action.

optical and electronic properties, and enable the optical readout of the information.^[51] The successful isolation of robust in-plane ferroelectricity in vdW hybrid perovskite lays the groundwork for all the tantalizing possibilities.

Experimental Section

Sample Preparation and Characterization: Stoichiometric amount of lead chloride and benzylammonium chloride was first dissolved in a concentrated HCl aqueous solution. Small single crystals of BA_2PbCl_4 were then obtained by slow evaporation of the solution at room temperature. The single crystals were plate-like with the plane parallel to the 2D layers. The crystals were then mechanically exfoliated onto different substrates using the Scotch tape method. The morphology and thickness of the obtained thin flakes were scrutinized by optical microscope and AFM. The phase purity and crystallinity of the crystals were verified using high-resolution XRD (Rigaku SmartLab). The vibrational spectroscopies were collected by FTIR (PerkinElmer Spectrum GX) and confocal Raman (Witec alpha300).

PFM and Ferroelectric Polarization Measurement: PFM measurement was carried out on a commercial AFM (Asylum Research MFP-3D) using a soft AFM tip with a spring constant of $\approx 0.2 \text{ N m}^{-1}$ (CONTPt, NanoWorld), to prevent sample surface damage. To enhance the signal-to-noise ratio, resonance-enhanced DART model^[52] was used, with the tip driven with an AC voltage of 1–2 V at the lateral contact resonance ($\approx 220 \text{ kHz}$). The torsional inverse optical lever sensitivity (nm V^{-1}) was calibrated using combined Sader method and thermal noise method^[53] to obtain quantitative piezoelectric displacement data (Figure S11 and Text S2, Supporting Information). Angular-resolved lateral PFM was performed at different azimuth angles between the sample and AFM cantilever.

Device Fabrication and Measurement: For in-plane switching devices, Au or Pt planar electrodes were defined by standard photolithography, thermal evaporation of metal, and lift-off process. Then the targeted flakes were transferred onto the electrode channel using dry method. Interdigitated electrodes and PET devices were patterned through

a shadow mask. Ferroelectric domain switching and polarization measurements were performed using a commercial ferroelectric tester (Radiant Technologies Multi ferroic). Electrical measurements of the piezoelectric flexible devices were measured by Agilent B1500A Semiconductor Device Analyzer.

Supporting Information

Supporting Information is available from the Wiley Online Library or from the author.

Acknowledgements

L.Y. and F.L. contributed equally to this work. L.Y. and J.W. acknowledge financial support from the Ministry of Education, Singapore under projects AcRF Tier 1 RG126/14 and RG 99/16. Z.L. acknowledges the support from the Singapore National Research Foundation under NRF award number NRF-NRFF2013-08 and the Ministry of Education, Singapore under project Tier 2 MOE2016-T2-2-136.

Conflict of Interest

The authors declare no conflict of interest.

Keywords

2D materials, ferroelectricity, flexible electromechanical devices, hybrid perovskite, piezoresponse force microscopy

Received: May 22, 2018

Revised: September 4, 2018

Published online: October 17, 2018

- [1] L. Seixas, A. S. Rodin, A. Carvalho, A. H. Castro Neto, *Phys. Rev. Lett.* **2016**, *116*, 206803.
- [2] M. Wu, X. C. Zeng, *Nano Lett.* **2016**, *16*, 3236.
- [3] C. Gong, L. Li, Z. Li, H. Ji, A. Stern, Y. Xia, T. Cao, W. Bao, C. Wang, Y. Wang, Z. Q. Qiu, R. J. Cava, S. G. Louie, J. Xia, X. Zhang, *Nature* **2017**, *546*, 265.
- [4] B. Huang, G. Clark, E. Navarro-Moratalla, D. R. Klein, R. Cheng, K. L. Seyler, D. Zhong, E. Schmidgall, M. A. McGuire, D. H. Cobden, W. Yao, D. Xiao, P. Jarillo-Herrero, X. Xu, *Nature* **2017**, *546*, 270.
- [5] J. Junquera, P. Ghosez, *Nature* **2003**, *422*, 506.
- [6] H. Lu, X. Liu, J. D. Burton, C. W. Bark, Y. Wang, Y. Zhang, D. J. Kim, A. Stamm, P. Lukashev, D. A. Felker, C. M. Folkman, P. Gao, M. S. Rzechowski, X. Q. Pan, C. B. Eom, E. Y. Tsymlal, A. Gruverman, *Adv. Mater.* **2012**, *24*, 1209.
- [7] P. Yu, W. Luo, D. Yi, J. X. Zhang, M. D. Russell, C.-H. Yang, L. You, G. Singh-Bhalla, S. Y. Yang, Q. He, Q. M. Ramasse, R. Erni, L. W. Martin, Y. H. Chu, S. T. Pantelides, S. J. Pennycook, R. Ramesh, *Proc. Natl. Acad. Sci.* **2012**, *109*, 9710.
- [8] F. Liu, L. You, K. L. Seyler, X. Li, P. Yu, J. Lin, X. Wang, J. Zhou, H. Wang, H. He, S. T. Pantelides, W. Zhou, P. Sharma, X. Xu, P. M. Ajayan, J. Wang, Z. Liu, *Nat. Commun.* **2016**, *7*, 12357.
- [9] K. Chang, J. Liu, H. Lin, N. Wang, K. Zhao, A. Zhang, F. Jin, Y. Zhong, X. Hu, W. Duan, Q. Zhang, L. Fu, Q.-K. Xue, X. Chen, S.-H. Ji, *Science* **2016**, *353*, 274.
- [10] W.-Q. Liao, Y. Zhang, C.-L. Hu, J.-G. Mao, H.-Y. Ye, P.-F. Li, S. D. Huang, R.-G. Xiong, *Nat. Commun.* **2015**, *6*, 7338.
- [11] H.-Y. Ye, W.-Q. Liao, C.-L. Hu, Y. Zhang, Y.-M. You, J.-G. Mao, P.-F. Li, R.-G. Xiong, *Adv. Mater.* **2016**, *28*, 2579.
- [12] C. C. Stoumpos, D. H. Cao, D. J. Clark, J. Young, J. M. Rondinelli, J. I. Jang, J. T. Hupp, M. G. Kanatzidis, *Chem. Mater.* **2016**, *28*, 2852.
- [13] W. Li, A. Thirumurugan, P. T. Barton, Z. Lin, S. Henke, H. H. M. Yeung, M. T. Wharmby, E. G. Bithell, C. J. Howard, A. K. Cheetham, *J. Am. Chem. Soc.* **2014**, *136*, 7801.
- [14] W. Wu, L. Wang, Y. Li, F. Zhang, L. Lin, S. Niu, D. Chenet, X. Zhang, Y. Hao, T. F. Heinz, J. Hone, Z. L. Wang, *Nature* **2014**, *514*, 470.
- [15] M. Kim, J. Im, A. J. Freeman, J. Ihm, H. Jin, *Proc. Natl. Acad. Sci.* **2014**, *111*, 6900.
- [16] M. Kepenekian, R. Robles, C. Katan, D. Sapor, L. Pedesseau, J. Even, *ACS Nano* **2015**, *9*, 11557.
- [17] K. S. Novoselov, D. Jiang, F. Schedin, T. J. Booth, V. V. Khotkevich, S. V. Morozov, A. K. Geim, *Proc. Natl. Acad. Sci.* **2005**, *102*, 10451.
- [18] A. Gannepalli, D. G. Yablon, A. H. Tsou, R. Proksch, *Nanotechnology* **2011**, *22*, 355705.
- [19] S. Elisabeth, *J. Phys. D: Appl. Phys.* **2011**, *44*, 464003.
- [20] P. Maksymovych, M. Huijben, M. Pan, S. Jesse, N. Balke, Y.-H. Chu, H. J. Chang, A. Y. Borisevich, A. P. Baddorf, G. Rijnders, D. H. A. Blank, R. Ramesh, S. V. Kalinin, *Phys. Rev. B* **2012**, *85*, 014119.
- [21] M. Davis, M. Budimir, D. Damjanovic, N. Setter, *J. Appl. Phys.* **2007**, *101*, 054112.
- [22] Y. Kim, C. Bae, K. Ryu, H. Ko, Y. K. Kim, S. Hong, H. Shin, *Appl. Phys. Lett.* **2009**, *94*, 032907.
- [23] V. K. Sergei, K. Yuneok, D. F. Dillon, N. M. Anna, *Rep. Prog. Phys.* **2018**, *81*, 036502.
- [24] A. V. Ievlev, D. O. Alikin, A. N. Morozovska, O. V. Varenky, E. A. Eliseev, A. L. Kholkin, V. Y. Shur, S. V. Kalinin, *ACS Nano* **2015**, *9*, 769.
- [25] H. Lu, T. Li, S. Poddar, O. Goit, A. Lipatov, A. Sinitskii, S. Ducharme, A. Gruverman, *Adv. Mater.* **2015**, *27*, 7832.
- [26] R. Yang, Y. Qin, C. Li, L. Dai, Z. L. Wang, *Appl. Phys. Lett.* **2009**, *94*, 022905.
- [27] H. Zhu, Y. Wang, J. Xiao, M. Liu, S. Xiong, Z. J. Wong, Z. Ye, Y. Ye, X. Yin, X. Zhang, *Nat. Nanotechnol.* **2015**, *10*, 151.
- [28] K.-A. N. Duerloo, M. T. Ong, E. J. Reed, *J. Phys. Chem. Lett.* **2012**, *3*, 2871.
- [29] M. N. Blonsky, H. L. Zhuang, A. K. Singh, R. G. Hennig, *ACS Nano* **2015**, *9*, 9885.
- [30] J. M. Frost, K. T. Butler, F. Brivio, C. H. Hendon, M. van Schilfgarde, A. Walsh, *Nano Lett.* **2014**, *14*, 2584.
- [31] A. Stroppa, D. Di Sante, P. Barone, M. Bokdam, G. Kresse, C. Franchini, M.-H. Whangbo, S. Picozzi, *Nat. Commun.* **2014**, *5*, 5900.
- [32] S. Liu, F. Zheng, N. Z. Koocher, H. Takenaka, F. Wang, A. M. Rappe, *J. Phys. Chem. Lett.* **2015**, *6*, 693.
- [33] F. Zheng, H. Takenaka, F. Wang, N. Z. Koocher, A. M. Rappe, *J. Phys. Chem. Lett.* **2015**, *6*, 31.
- [34] Y. Kutes, L. Ye, Y. Zhou, S. Pang, B. D. Huey, N. P. Padture, *J. Phys. Chem. Lett.* **2014**, *5*, 3335.
- [35] Z. Fan, J. Xiao, K. Sun, L. Chen, Y. Hu, J. Ouyang, K. P. Ong, K. Zeng, J. Wang, *J. Phys. Chem. Lett.* **2015**, *6*, 1155.
- [36] H.-S. Kim, S. K. Kim, B. J. Kim, K.-S. Shin, M. K. Gupta, H. S. Jung, S.-W. Kim, N.-G. Park, *J. Phys. Chem. Lett.* **2015**, *6*, 1729.
- [37] G. Sharada, P. Mahale, B. P. Kore, S. Mukherjee, M. S. Pavan, C. De, S. Ghara, A. Sundaresan, A. Pandey, T. N. Guru Row, D. D. Sarma, *J. Phys. Chem. Lett.* **2016**, *7*, 2412.
- [38] M. S. Alvar, M. Kumar, P. W. M. Blom, G.-J. A. H. Wetzelaer, K. Asadi, *AIP Adv.* **2017**, *7*, 095110.
- [39] Y. Rakita, O. Bar-Elli, E. Meirzadeh, H. Kaslasi, Y. Peleg, G. Hodes, I. Lubomirsky, D. Oron, D. Ehre, D. Cahen, *Proc. Natl. Acad. Sci.* **2017**, *114*, E5504.
- [40] H. Rohm, T. Leonhard, M. J. Hoffmann, A. Colmann, *Energy Environ. Sci.* **2017**, *10*, 950.
- [41] E. Strelcov, Q. Dong, T. Li, J. Chae, Y. Shao, Y. Deng, A. Gruverman, J. Huang, A. Centrone, *Sci. Adv.* **2017**, *3*, e1602165.
- [42] M. Ahmadi, L. Collins, A. Puzetzy, J. Zhang, J. K. Keum, W. Lu, I. Ivanov, S. V. Kalinin, B. Hu, *Adv. Mater.* **2018**, *30*, 1705298.
- [43] Z. Sun, X. Liu, T. Khan, C. Ji, M. A. Asghar, S. Zhao, L. Li, M. Hong, J. Luo, *Angew. Chem., Int. Ed.* **2016**, *55*, 6545.
- [44] H. Tsai, W. Nie, J.-C. Blancon, C. C. Stoumpos, R. Asadpour, B. Harutyunyan, A. J. Neukirch, R. Verduzco, J. J. Crochet, S. Tretiak, L. Pedesseau, J. Even, M. A. Alam, G. Gupta, J. Lou, P. M. Ajayan, M. J. Bedzyk, M. G. Kanatzidis, A. D. Mohite, *Nature* **2016**, *536*, 312.
- [45] L. Li, Z. Sun, P. Wang, W. Hu, S. Wang, C. Ji, M. Hong, J. Luo, *Angew. Chem., Int. Ed.* **2017**, *56*, 12150.
- [46] D. Di Sante, P. Barone, R. Bertacco, S. Picozzi, *Adv. Mater.* **2013**, *25*, 509.
- [47] A. Manchon, H. C. Koo, J. Nitta, S. M. Frolov, R. A. Duine, *Nat. Mater.* **2015**, *14*, 871.
- [48] J. R. Schaibley, H. Yu, G. Clark, P. Rivera, J. S. Ross, K. L. Seyler, W. Yao, X. Xu, *Nat. Rev. Mater.* **2016**, *1*, 16055.
- [49] D. B. Mitzi, *Prog. Inorg. Chem.* **2007**, *48*, 1.
- [50] L. Pedesseau, D. Sapor, B. Traore, R. Robles, H.-H. Fang, M. A. Loi, H. Tsai, W. Nie, J.-C. Blancon, A. Neukirch, S. Tretiak, A. D. Mohite, C. Katan, J. Even, M. Kepenekian, *ACS Nano* **2016**, *10*, 9776.
- [51] R. Guo, L. You, Y. Zhou, Z. Shih Lim, X. Zou, L. Chen, R. Ramesh, J. Wang, *Nat. Commun.* **2013**, *4*, 1990.
- [52] J. R. Brian, C. Clint, V. K. Sergei, P. Roger, *Nanotechnology* **2007**, *18*, 475504.
- [53] K. Wagner, P. Cheng, D. Vezhenov, *Langmuir* **2011**, *27*, 4635.